UiO-66 derived etched carbon/polymer membranes: High-performance supports for the extraction of organic pollutants from water

Carlos Palomino Cabello, Maria Francesca Font Picó, Fernando Maya, Mateo del Rio, Gemma Turnes Palomino**

*Department of Chemistry, University of the Balearic Islands, Palma de Mallorca, E-07122, Spain. *E-mail: carlos.palomino@uib.es; g.turnes@uib.es Fax: (+34) 971 173426. Phone: (+34) 971 173389.*

ABSTRACT

Herein we report the use of the zirconium metal-organic framework (UiO-66) as precursor to prepare porous carbons by a direct carbonization step (carbon-ZrO_2). By applying a post-carbonization acidic etching treatment with hydrofluoric acid (HF), the initial surface area of the carbon-ZrO_2 sample increased from 270 m^2 g^{-1} to 1550 m^2 g^{-1} (carbon-ZrO_2-HF). This increase is attributed to the partial removal of the ZrO_2 present in the UiO-66-derived carbon. Carbon-ZrO_2-HF exhibited fast adsorption kinetics and an outstanding maximum adsorption capacity of 510 mg g^{-1} for the dye rhodamine B. For practical applications, the obtained porous carbon-ZrO_2-HF material was used to fabricate a carbon composite membrane using polyvinylidene fluoride. The prepared membranes were applied as water filtration supports for the extraction of toxic phenols from water, including an endocrine disrupting phenol with widespread exposure: bisphenol A. High efficiency for the simultaneous extraction of phenolic pollutants, and an excellent reusability with a variation of a 2% for 10 consecutive bisphenol A extraction cycles, were obtained. Due to their high and accessible porosity, small particles size, and facile processability into membranes, the UiO-66 derived etched carbons are promising materials for environmental applications, such as the extraction of organic toxic pollutants.

Keywords: Metal-organic frameworks; nanoporous carbons; membranes; flow-through support; etching; pollutant extraction

1. Introduction

Metal-organic frameworks (MOFs) have gained particular attention as a novel class of nanoporous materials due to their varied architectures, built from metal ion (or clusters) with bridging organic ligands, high surface areas, adjustable pore sizes from the microporous to the mesoporous scale, and tailored chemical functionalities [1-5]. Due to these properties, MOFs have been widely studied as materials for catalysis [6,7], gas storage [8,9], sensing [10], drug delivery [11], and, more recently, for the adsorptive removal of different pollutants, such as heavy metals, dyes, or phenols [12-15]. In this field, one of the most important barriers in the applicability of MOFs as sorbents is their limited stability in aqueous or complex mediums. In this regard, MOFs have recently shown to be useful precursors for the synthesis of other materials, such as metal oxides, metal carbides, or porous carbons [16-18]. Specifically, MOFs-derived porous carbons have attracted much attention because the periodic porous and hybrid structure of MOFs provides unique features for the fabrication of porous carbons with uniform pores of different sizes and with novel structures and properties. In addition, considering the large carbon content of organic components in MOFs, highly porous carbons can be achieved by a very simple, one-step pathway, without the need of any additional carbon precursor, avoiding tedious, costly and environmentally harmful synthetic procedures [19-21]. Thermal carbonization of MOFs is carried out in an inert atmosphere in which the organic linkers and metal ions are transformed into carbonaceous structures and metal or metal oxide nanoparticles, respectively. The direct MOF carbonization process results, in this way, in the formation of metal- or metal oxide-carbon composite materials, where the precursor MOFs has a dual function acting as a sacrificial template and carbon precursor.

Thus far, several types of MOFs have been used as precursors to yield porous carbons for a wide range of applications, such as gas adsorption [22,23], catalysis [24,25], and electrochemical

energy storage [17,21]. In addition to these applications, MOF-derived porous carbon, due to their remarkable high surface area, thermal and chemical stability, and their tendency to interact with aromatic compounds, have acquired great significance as sorbents for the removal of chemical pollutants. For instance, ZIF-67 is an excellent precursor to obtain nanoporous carbons because their direct carbonization yields a magnetic porous carbon, which has been applied to the extraction of methylene blue dye [26], phenylurea herbicides [27] and benzoylurea insecticides [28]. The potential of ZIF-8-derived nanoporous carbon as sorbent has also been studied and demonstrated for the extraction of carbamate pesticides by Hao et al. [29] Other examples of the application of MOFs-derived carbons as pollutant sorbents are the use of bimetallic ZIF-derived carbons, containing both Zn(II) and Co(II), for the extraction of chlorophenols and sex hormones in water samples [30,31] and the application of porous carbon derived from metal azolate framework-6 for removal of different pharmaceuticals and personal care products in water [32]. Very recently, the first examples of the use of porous carbon prepared from Zr-based MOF as sorbent of organic pollutants have been reported [33,34]. Among the different types of Zr-based MOFs synthesized so far, UiO-66, which is a cubic rigid porous MOF based on a $Zr_6O_4(OH)_4$ clusters linked by 1,4-benzenedicarboxylate [35], has received much attention because of its thermal stability, tunable pore size, and high specific surface area [36-38], being a promising precursor for the synthesis of nanoporous carbons.

A critical step in the direct application of porous materials for pollutant extraction is the post-extraction retrieval of the sorbent from the sample medium, which requires laborious and, in most cases, incomplete filtration and centrifugation steps. An interesting alternative to solve this limitation is the integration of the porous materials into functional extraction devices, such as beads [39,40], fibers [34,41], monoliths [42,43], and membranes [44,45], facilitating their use as sorbents

for the extraction of pollutants from water with environmental or monitoring purposes. Among them, the incorporation of porous solids in membranes is a desirable approach due to their reusability and excellent flow-through properties achieving high extraction yields, and the easy automation of the process, increasing the extraction throughput and reproducibility.

Bearing these in mind, we report the first example of the application of MOF-derived porous carbon/polymer membranes as sorbents for the extraction of environmental organic pollutants from water. As a proof of concept, UiO-66 was used as a precursor and a template for the preparation of porous carbon/ZrO_2 composite material (carbon-ZrO_2) by one-step direct carbonization process. A post-carbonization acidic etching treatment was carried out to increase the porosity of the material. The resulting porous carbon (carbon-ZrO_2-HF) was then immobilized in a Nylon filter using polyvinylidene fluoride as binder, obtaining a highly robust an efficient flow-through support for pollutant extraction. Rhodamine B was selected as model organic dye to evaluate the performance of the prepared MOF-derived carbon/polymer membranes. Additionally, we used these composite membranes for the flow-through extraction of four substituted phenols (1-naphthol (NPh), 2,4-dimethylphenol (2,4-DMP), 2,4-dichlorophenol (2,4-DCP) and bisphenol A (BPA)), with representative structures of the vast family of phenols catalogued as environmental pollutants due to their widespread use as pharmaceuticals, personal care products, or as by-products from massively used plastics [46].

2. Experimental

2.1. Chemicals

Methanol (≥99.8%), ethanol (96%), N,N-dimethylformamide (DMF, 99.5%), terephthalic acid (99%), hydrofluoric acid (HF, 40%), acetone (≥99.8%), 1-naphthol (NPh, 99%), and charcoal activated powder (reagent grade ref, Ca0352, 930 $m^2 g^{-1}$), were obtained from Scharlau. Zirconium (IV) chloride ($ZrCl_4$, 98%), and rhodamine B (≥98%) were acquired from ACROS. Polyvinylidene difluoride (PVDF, MW ~ 180,000), 2,4-dimethylphenol (2,4-DMP, 98%), 2,4-dichlorophenol (2,4-DCP, 98%), and bisphenol A (BPA, 97%) were obtained from Sigma & Aldrich. As starting support, GVS Maine Magna 0.45 μm Nylon membrane filters (25 mm diameter and 80 μm thickness) were used.

A stock standard solution of each selected phenol (2000 mg L^{-1}) was prepared in methanol. A working solution with a concentration of 10 mg L^{-1} of each phenol was prepared daily by diluting the stock standard solution in water. A standard mixture of phenols (10 mg L^{-1}) was prepared in water. All solutions were prepared using Milli-Q water (Direct-8 purification system, resistivity >18 MΩ cm, Millipore Iberica, Spain).

2.2. Characterization

Powder X-ray diffraction (XRD) data were collected using CuKα (λ = 1.5418 Å) radiation on a Bruker D8 Advance diffractometer. The morphology and elemental distribution of the prepared materials were analyzed by using a scanning electron microscope (Hitachi S-3400N), equipped with a Bruker AXS Xflash 4010 EDS system to enable multielemental mapping, and transmission electron microscope (Hitachi ABS) operated at 100 kV. Nitrogen adsorption-desorption isotherms were measured at 77 K using a TriStar II (Micromeritics) gas adsorption analyzer. The samples were previously outgassed at 393 K overnight. Data were analyzed by using the Brunauer-Emmett-Teller model (BET) to determine the specific surface area. The pore volume and pore size distribution were calculated using the two dimensional non local density functional theory model

(2D-NLDFT). Thermogravimetric analysis (TGA) was carried out in an air atmosphere using a TA Instrument SDT 2960 simultaneous DSC-TGA.

2.3. Preparation of carbon-ZrO_2 sample.

Zirconium-based metal-organic framework (UiO-66) was prepared by solvothermal reaction according to a procedure reported in the literature [47]. 1.0 mmol of $ZrCl_4$, 1.0 mmol of terephthalic acid and 12 ml of DMF were mixed in a Teflon-lined stainless steel autoclave and kept at 393 K for 24 h. The resulting white solid was washed with ethanol and vacuum dried. Carbon-ZrO_2 sample was obtained from UiO-66 crystals via carbonization in a tubular furnace under N_2 atmosphere at 1073 K (heating rate of 2 K min^{-1}) for 3 h (**Fig. 1a**).

2.4. Preparation of carbon-ZrO_2-HF sample.

A portion of the carbon-ZrO_2 sample was etched with 1.0 M HF aqueous solution at room temperature for 24 h, washed thoroughly with water and dried at 333 K (**Fig. 1a**).

2.5. Preparation of carbon-ZrO_2-HF membranes.

Carbon-ZrO_2-HF membranes were prepared adapting a previously reported procedure [48]. 150 mg of dry carbon-ZrO_2-HF powder was dispersed in 5 ml of acetone by sonicating for 30 min. The so obtained suspension was mixed with 1.0 g of PVDF dissolved in DMF (7.5 wt. %) and sonicated for another 30 min. Then, the acetone was evaporated under a stream of pure nitrogen gas, and the resulting concentrated carbon-PVDF dispersion in DMF was casted onto three Nylon membranes. The prepared composite materials were heated at 333 K for 1 h to remove the DMF and, before their use for further experiments, they were conditioned by flushing them with methanol and water (**Fig. 1b**). Blank PVDF and commercial carbon membranes were prepared as reference materials following the same procedure.

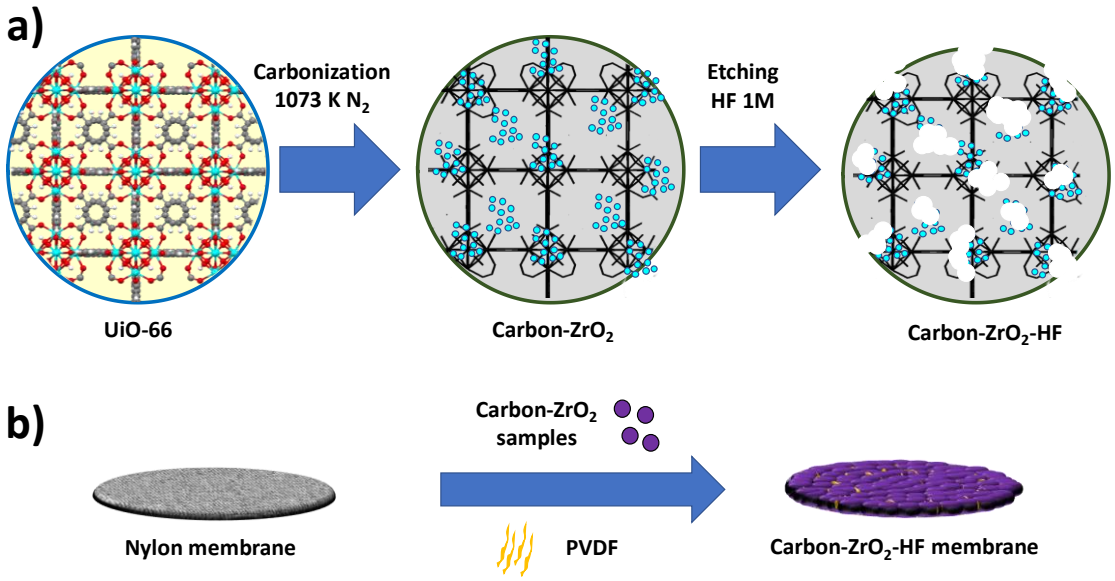

Fig. 1. Schematic representation of the preparation of (a) carbon-ZrO_2 and carbon-ZrO_2-HF samples using UiO-66 as a precursor and (b) carbon-ZrO_2-HF membrane supported on a Nylon filter

2.6. Extraction procedure in batch conditions

All extraction experiments were performed with 1 mg of sample (carbon-ZrO_2 or carbon-ZrO_2-HF) per ml of rhodamine B aqueous solution. The concentration of remaining rhodamine B in solution after extraction was measured using UV-Vis spectrophotometry (553 nm). For kinetics studies, 10 mg L^{-1} rhodamine B aqueous solution were mixed with the adsorbent under stirring, and the extracted amount of the dye was measured at predetermined intervals of time. Adsorption isotherm experiments were conducted in a concentration range of 25-800 mg L^{-1} of rhodamine B during 24 h to ensure that equilibrium conditions were reached.

2.7. Analysis of the adsorption data

The adsorption data of kinetics studies were analyzed with a pseudo-second-order adsorption model [49,50], whose linearized-integral form is expressed by the following equation:

$$\frac{t}{q_t} = \frac{t}{q_e} + \frac{1}{k_2 q_e^2}$$

where, q_t and q_e (mg g^{-1}) are the amount of dye adsorbed at a time t (min) and at equilibrium, respectively, and k_2 is the pseudo-second-order rate constant (g mg^{-1} min^{-1}).

The maximum adsorption capacity was determined using the linearized form of the Langmuir equation, which is commonly represented as:

$$\frac{C_e}{q_e} = \frac{C_e}{q_{max}} + \frac{1}{q_{max} k}$$

where C_e (mg L^{-1}) is the remaining dye concentration at equilibrium, q_e (mg g^{-1}) is the amount of dye adsorbed at equilibrium (mg g^{-1}), q_{max} is the maximum adsorption capacity (mg g^{-1}), and k is the Langmuir constant (L mg^{-1}).

2.8. Breakthrough experiments

For the breakthrough experiments, a solution of rhodamine B (2 mg L^{-1}) was filtered through the different membranes prepared in a vacuum filtration system. The outlet samples were collected and analyzed by UV-visible spectroscopy to determine the extracted amount of rhodamine B.

2.9. Extraction of phenols

The extraction properties of the prepared membranes were examined using different phenolic compounds. An aqueous solution of the corresponding phenol (10 mg L^{-1}) was passed through the

membrane and the quantification of the remaining amount of phenol in the aqueous phase was determined by UV-visible spectroscopy. Following the same procedure, the extraction capacity of the membranes using a standard mixture of phenols was studied.

3. Results and discussion

3.1. Preparation and characterization of porous carbon-ZrO_2 and carbon-ZrO_2-HF

For the preparation of the porous carbon-ZrO_2 composite material, first we synthesized the precursor UiO-66 metal-organic framework followed by one-step direct carbonization of the MOF at 1073 K under N_2 atmosphere. The so prepared carbon was treated with HF to obtain the carbon-ZrO_2-HF sample. The powder X-ray diffraction pattern of the UiO-66 precursor (**Fig. S1**) showed good crystallinity and was in good agreement with the XRD pattern previously reported for the same MOF [38]. **Fig. 2a s**hows the X-ray powder patterns of both, carbon-ZrO_2 and carbon-ZrO_2-HF, samples. After the carbonization process, the sharp diffraction peaks corresponding to UiO-66 are no longer observed, while four broad new peaks appear, which are assigned to tetragonal ZrO_2 (JCPDS no. 80-0965). As demonstrated the lower intensity of the peaks corresponding to tetragonal ZrO_2 present in the X-ray diffraction pattern of carbon-ZrO_2-HF, with respect to those present in the XRD diffractogram of carbon-ZrO_2 sample (**Fig. 2a**), part of the ZrO_2 nanoparticles were removed by chemical etching. In addition, new diffraction lines were observed, which were attributed to the monoclinic phase of the ZrO_2 (JCPDS no. 83-0944), indicating the coexistence of both, monoclinic and tetragonal, phases in the porous carbon [51]. After removing ZrO_2 nanoparticles by HF aqueous solution, broad peaks corresponding to carbon signals can be also

observed at 2θ= 13°, 24° and 43°, suggesting the formation of a graphitic carbon structure [19,20,26].

To study the morphology of the obtained porous carbons, they were characterized by scanning electron microscopy (**Fig. 2b** and **Fig. 2c)** and transmission electron microscopy (**Fig. 2d** and **Fig. 2e**) before and after HF treatment. Compared to the initial UiO-66 (**Fig. S2**), both, carbon-ZrO_2 and carbon-ZrO_2-HF, samples retained the original globular shape of the parent UiO-66. However, although the obtained carbons retained the original morphology of the precursor MOF, their average crystal size decreased from 250 nm (UiO-66) to 160 nm in both cases, due to shrinkage which takes place during the carbonization process [26,52]. TEM images showed that, after acid treatment, the ZrO_2 nanoparticles were almost totally removed from the carbon matrix.

Nitrogen sorption experiments were performed to study the porosity of the prepared materials. Before carbonization, the UiO-66 precursor (**Fig. S3**) exhibit typical type I(a) isotherm of the IUPAC classification with a drastic increment of the N_2 uptake at low relative pressure, which is indicative of the presence of micropores. After carbonization, carbon-ZrO_2 sample displayed a similar type isotherm to that of the precursor UiO-66 but with a much lower nitrogen uptake at low relative pressures (**Fig. 2f**), which is probably due to the partial collapse of the structure during the carbonization process. Although the BET surface area and total pore volume decreases considerably after the carbonization process, the carbon-ZrO_2 sample still possess a high surface area and total pore volume of 270 $m^2\ g^{-1}$ and 0.104 $cm^3\ g^{-1}$, respectively (**Table 1**). The pore size distribution, calculated using the 2D-NLDFT model (**Fig. S4**), showed that most of the pores have a diameter of 9 Å, while a small amount of pores have larger pore sizes between 15 and 20 Å. After the acid treatment, the total amount of adsorbed nitrogen increased drastically (**Fig. 2f**), which, in agreement with XRD and TEM results, is probably due to the removal of part

of the ZrO_2 nanoparticles by HF etching [19,20]. The specific surface area calculated using the BET equation and the total pore volume were 1550 m^2 g^{-1} and 0.762 cm^3 g^{-1}, respectively. The isotherms for carbon-ZrO_2-HF sample corresponds a type I(b) of IUPAC classification with a steep increase of the nitrogen adsorbed volume at low relative pressure, followed by a moderate slope at intermediate pressures, which indicates the combined presence of micropores and mesopores. This hierarchical pore system was consistent with the pore size distribution obtained (**Fig. S5**), which showed that, although most of the pores still has a diameter in the range of 8-11 Å, the fraction of wider pores, with diameters between 15 and 34 Å, increases after the acid treatment.

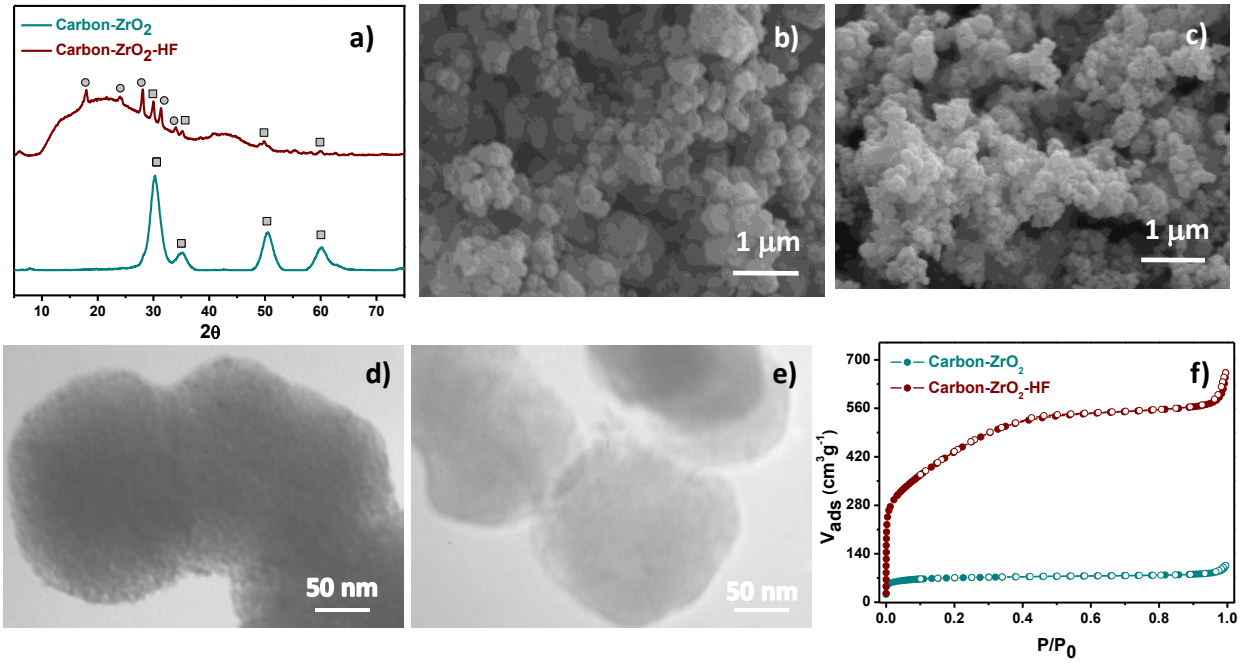

Fig. 2. (a) XRD pattern of the prepared carbon-ZrO_2 samples. Peaks: Tetragonal ZrO_2 (squares), monoclinic ZrO_2 (circles). SEM images of (b) carbon-ZrO_2 and (c) carbon-ZrO_2-HF samples. TEM images of (d) carbon-ZrO_2 and (e) carbon-ZrO_2-HF. (f) Nitrogen adsorption-desorption isotherms of the carbon-ZrO_2 samples.

Table 1. Sample textural properties and residual weight percentage after combustion

Sample	S_{BET} (m^2 g^{-1})	V_p (cm^3 g^{-1})	Pore width (Å)	Residual weight (%)
Carbon-ZrO_2	270	0.104	8-10 / 15-20	62.0
Carbon-ZrO_2-HF	1550	0.762	8-11 / 15-34	6.6

The partial removal of ZrO_2 nanoparticles with HF, which generates the additional porosity in carbon-ZrO_2-HF, was confirmed by the reduction of the residual weights values measured after heating carbon-ZrO_2 and carbon-ZrO_2-HF samples at 1073 K in air, which go from an initial value of 62.0 wt. %, for the carbon-ZrO_2 sample, to a value of just a 6.6 % after acid treatment (**Table 1**).

3.2. Extraction of rhodamine B under batch conditions

To check the adsorption capacity of the prepared materials, rhodamine B was selected as pollutant model for the extraction studies in batch conditions. **Fig. 3a** shows the percentage of rhodamine B (C_0= 10 mg L^{-1}) adsorbed by the two porous carbon samples at different time intervals. Both materials, carbon-ZrO_2 and carbon-ZrO_2-HF, exhibit a remarkable fast uptake of rhodamine B, reaching, after only 1 minute, a percentage of extraction of more than 99% and 80%, respectively. A pseudo-second-order non-linear kinetic model was used to fit the experimental results (**Fig. 3a**), obtaining, in both cases, correlation coefficients (R^2) of 0.999 (**Fig. S6**), which confirms that the kinetics of the adsorption process is well described by this model.

Isotherms of adsorption of rhodamine B on carbon-ZrO_2 and carbon-ZrO_2-HF samples were recorded at ambient temperature after a period of 24 h in order to ensure equilibrium conditions (**Fig. 3b)**. Langmuir plots (**Fig. S7**) were used to determine the maximum adsorption

capacity (q_{max}). The obtained correlation coefficients, were in both cases of 0.999, indicate that the adsorption process is well described by the Langmuir model [53], suggesting that the adsorption takes place at specific homogeneous sites within the adsorbent. Carbon-ZrO_2-HF sample has a maximum extraction capacity of rhodamine B of 510 mg g^{-1}, which is 3 times higher than that of the carbon-ZrO_2 sample (160 mg g^{-1}), and rank among the highest values of adsorption capacity of rhodamine B reported in the literature [54-58]. Considering the dimensions of the rhodamine B molecule [59], and according to the textural properties of the prepared materials (**Table 1**), the similarity of sizes between the rhodamine B and the pore diameter of carbon-ZrO_2 probably hinders the access of the molecules to the carbon pores limiting the quantity adsorbed. However, after acid treatment, the material possesses various pores in the mesoporous range, larger than the size of the molecules of rhodamine B, which can facilitate the adsorption of the rhodamine B in the pores, explaining the higher extraction capacity of the acid treated sample. Furthermore, the high degree of graphitization of the carbon-ZrO_2-HF sample could also contribute to the adsorption process allowing an effective interaction of the carbon surface with the aromatic rings of rhodamine B through π-π interactions [19,26,60].

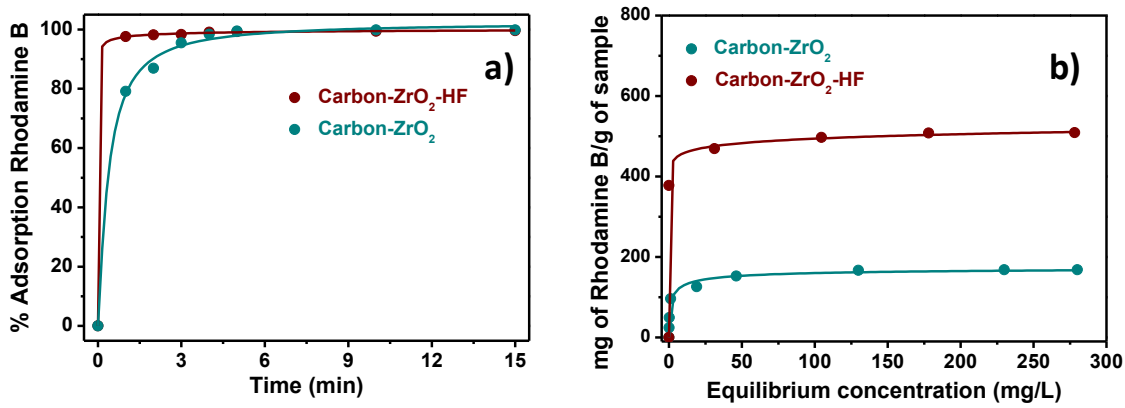

Fig. 3. (a) Time-dependent adsorption of rhodamine B (10 mg L^{-1}) using bulk carbon-ZrO_2 and carbon-ZrO_2-HF samples. Fits of pseudo-second order non-linear kinetic model to the experimental rhodamine B adsorption data are shown as solid lines. (b) Adsorption isotherms of rhodamine B on bulk carbon-ZrO_2 and carbon-ZrO_2-HF samples. Fits of Langmuir model to the experimental rhodamine B adsorption data are shown as solid lines.

3.3. Characterization of the carbon-ZrO_2-HF membranes

The prepared carbon materials showed to be promising sorbents for the extraction of rhodamine B from aqueous solutions, in particular that obtained by acid treatment of UiO-66 derived carbon (carbon-ZrO_2-HF), which, due to its superior extraction capacity, was chosen for further experiments. However, one of the most important limitations of the use of a sorbent, based on small particles dispersed in the extraction medium, is the tedious and difficult sorbent retrieval step. In order to overcome this drawback, and also explore the adsorption flow-through properties of the carbon-ZrO_2-HF sample, polymer membranes containing this material were prepared. Membranes for pollutant extraction were obtained by coating a commercially available Nylon filter with a homogeneous carbon-ZrO_2-HF/PVDF dispersion. Characterization results of the etched-carbon membranes are shown in **Fig. 4**. **Fig. 4a** shows the XRD diffraction patterns of a

Nylon membrane in the absence and the presence of the porous carbon-ZrO_2-HF/PVDF coating. It can be observed that, after the coating of the membrane with the carbon, the intensity of original peaks due to the Nylon significantly decreases, while new X-ray diffraction lines appear which match well with those of the bulk carbon-ZrO_2-HF sample showed in **Fig. 2a**. **Figs. 4b and 4c** show SEM images of the Nylon filter before and after coating with the carbon-ZrO_2-HF/PVDF dispersion. After coating, the filter is completely covered with a dense layer of the porous carbon of approximately 140 µm of thickness, as can be observed in a cross-section SEM image of the composite material (**Fig. 4d**). A SEM micrograph at higher magnification of the carbon-ZrO_2-HF/PVDF membrane (**Fig. S8)** shows that the morphology of the etched-carbon particles was not modified. The presence of zirconium on the coated material was demonstrated by EDS, which showed an intense Zr band, (**Fig. 4e**) whereas no zirconium is detected in the original Nylon filter. In addition, elemental EDS mapping (**Fig. 4f**) showed the homogeneous distribution of zirconium on the membrane.

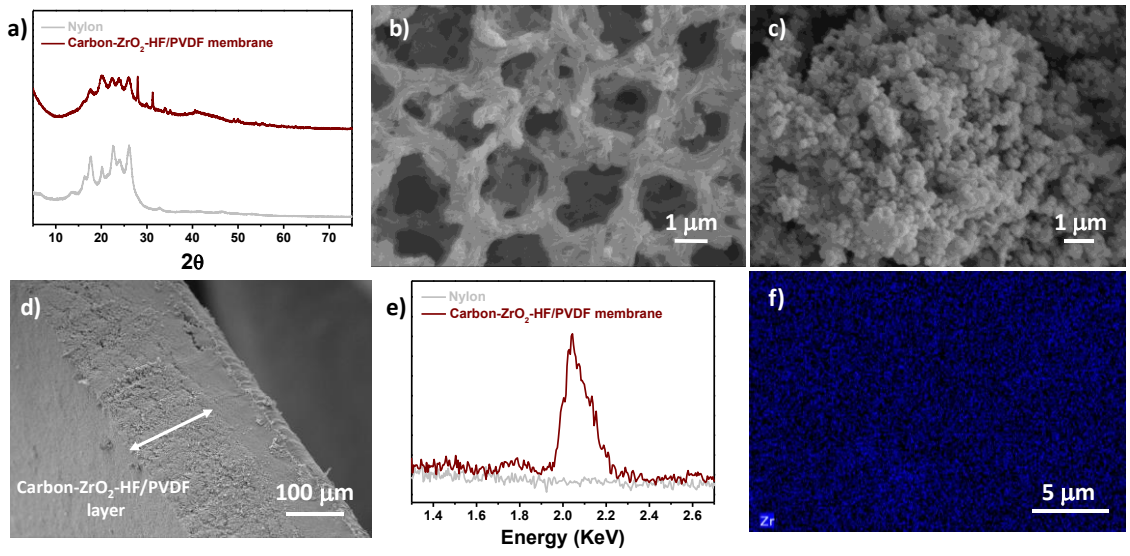

Fig. 4. (a) XRD patterns of a Nylon membrane before and after coating with the carbon-ZrO_2-HF/PVDF dispersion. Representative SEM images of the (b) bare Nylon and (c) carbon-ZrO_2-HF/PVDF coated

membranes. (d) Cross-section SEM micrograph of the carbon-ZrO_2-HF/PVDF coated membrane. (e) EDS spectra of the bare Nylon and the carbon-ZrO_2-HF/PVDF coated membranes. (f) EDS mapping of Zr of the carbon-ZrO_2-HF/PVDF membrane.

3.4. Breakthrough curves of rhodamine B adsorption on carbon-ZrO_2-HF/PVDF membranes

The breakthrough curves of adsorption of rhodamine B (**Fig. 5**) were obtained to evaluate the filtration adsorption performance of the prepared carbon-ZrO_2-HF/PVDF membranes using a vacuum filtration system. For comparison purposes a Nylon, a PVDF-coated Nylon membrane, and a porous carbon/PVDF membrane, prepared using a commercial activated carbon (930 $m^2 g^{-1}$) as carbon source, were also tested.

As shown in **Fig. 5** the breakthrough curve of the carbon-ZrO_2-HF/PVDF membrane exhibits a typical "S" shape with a large initial step of complete adsorption of rhodamine B due to the efficient mass transport through the pores of the membrane. The breakpoint on the breakthrough curve is the point when the concentration of the effluent from the membrane reaches a 5% of the initial concentration of the tested rhodamine B solution, which, in the case of the carbon-ZrO_2-HF/PVDF coated membrane, was reached after passing through the membrane 730 mL of the rhodamine B solution. In contrast, the breakpoints for the bare Nylon and the PVDF-coated Nylon membranes (**Fig. 5**) were reached after passing only 1.3 mL and 3.8 mL of rhodamine B solution, respectively, which indicates that the adsorption capacity of the carbon-ZrO_2-HF/PVDF coated membrane is mainly due to the presence of the porous etched-carbon. Compared to the membrane coated with the commercial carbon, the carbon-ZrO_2-HF/PVDF coated membrane allows the flow of a much larger volume (almost 75-fold larger) of rhodamine B solution before reaching the breakthrough point. After reaching the breakpoint of the carbon-ZrO_2-HF/PVDF membrane, the

concentration of rhodamine B in the effluent gradually increased, reaching the saturation point (defined as the point at which effluent concentration reaches nearly 100% of the initial concentration) after passing 1160 mL of rhodamine B dye solution, volume from which the membrane was completely saturated.

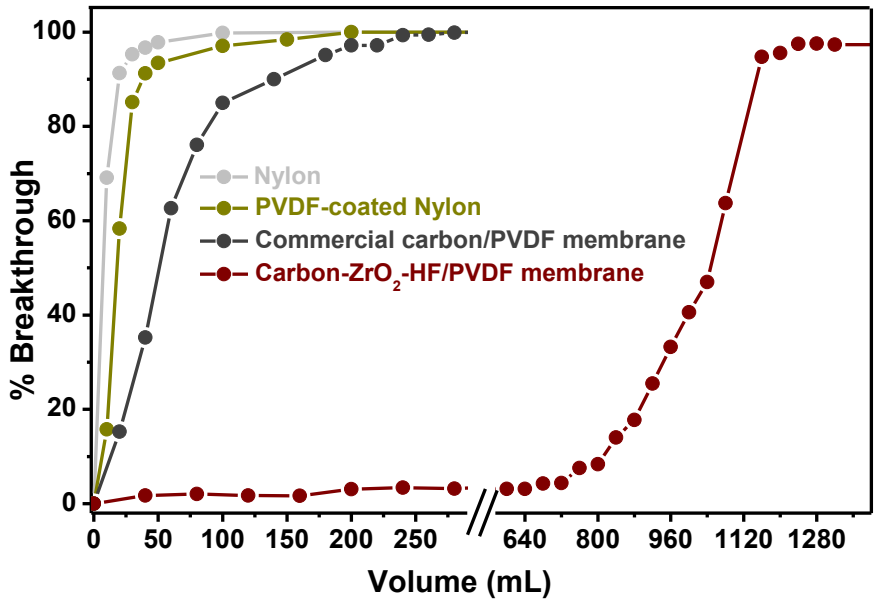

Fig. 5. Breakthrough curves of rhodamine B adsorption on bare Nylon and PVDF, commercial carbon/PVDF and carbon-ZrO_2-HF/PVDF coated membranes.

It should be also pointed out that, when comparing the flow rate of the bare Nylon and the PVDF-coated Nylon membrane, a large drop of the flow rate was observed after coating the Nylon membrane with the polymer, decreasing from 1500 L m^{-2} h^{-1} to just 225 L m^{-2} h^{-1} after coating. This decrease was attributed to the low permeability of the pure PVDF coating applied on top of the Nylon filter. However, after the incorporation of the carbon-ZrO_2-HF to the membrane, the

flow rate increased to 750 L m^{-2} h^{-1}, getting a high permeability combined with an outstanding pollutant extraction capacity.

3.5. Extraction of phenolic pollutants on UiO-66 derived etched-carbon/polymer membranes

In order to study the applicability of the carbon-ZrO_2-HF/PVDF membranes as adsorbent for the removal of other organic pollutants from water, phenolic pollutants of different size, hydrophobicity and functionality were selected (**Fig. S9**). Bisphenol A is a widespread plastic degradation by-product which exhibits estrogen-mimicking, hormone-like properties raising concern about its use in consumer products. The other three selected phenols are representative examples of typical phenolic pollutants containing additional aromatic rings (1-naphthol), halogen substituents (2,4-dichlorophenol), or alkyl groups (2,4-dimethylphenol). The performance of the carbon-ZrO_2-HF/PVDF membrane for the extraction of phenols was compared with the bare Nylon and PVDF-coated membranes (**Fig. 6a**). It can be observed that the carbon-ZrO_2-HF/PVDF membrane showed again a much higher extraction capacity than the membranes that did not contain the porous carbon, reaching the 100% of extraction for all the tested phenols. This improvement on phenols extraction performance is attributed, as in the case of the rhodamine B, to the existence of π-π interactions between the aromatic rings of the phenols and the carbon surface, as well as, the accessibility of all the compounds to the pores of the composite membrane.

To gain a deeper insight into the applicability of the prepared membranes for the extraction of water pollutants, and considering the coexistence of multiple pollutants in real water samples, a mixture containing simultaneously the four selected phenolic pollutants was filtered through the carbon-ZrO_2-HF/PVDF membrane. **Fig. 6b** shows the UV absorption spectra obtained for the phenols mixture standard solution, before and after extraction. Under the selected filtration conditions no presence of phenols was observed in the filtrate. However, after elution, an intense

absorbance was measured again, showing that the extracted phenol are easily and completely recovered, demonstrating the efficiency of the carbon-ZrO_2-HF/PVDF membrane for the extraction/recovery of mixtures of organic pollutants present in water samples.

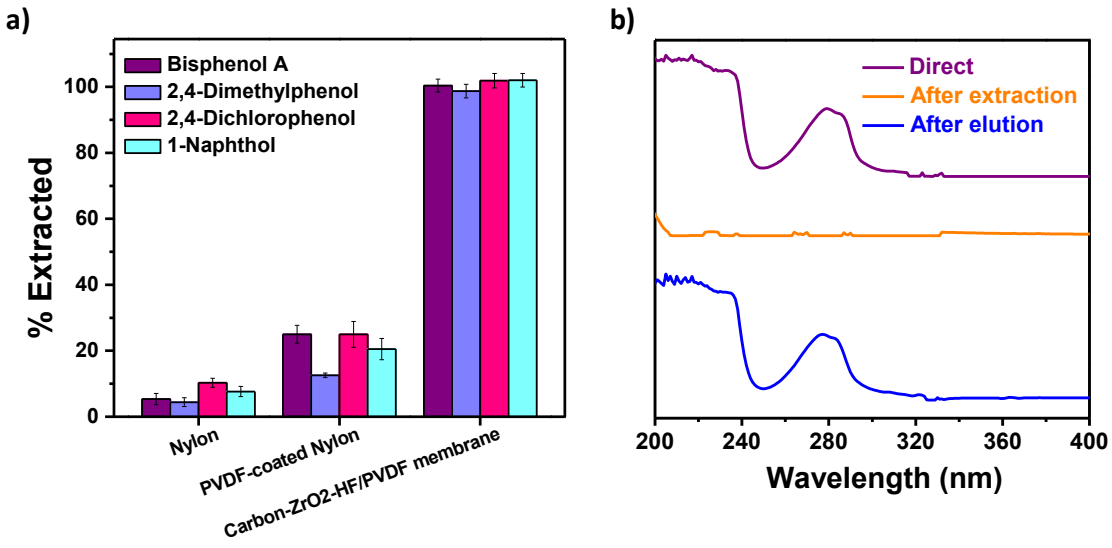

Fig. 6. (a) Amount of phenols extracted by using Nylon, PVDF and carbon-ZrO_2-HF/PVDF coated membranes. (b) UV-vis spectra of a phenolic compounds mixture solution before and after extraction with the carbon-ZrO_2-HF/PVDF membrane, and of the solution recovered after the elution with methanol.

The reusability of adsorbents is a crucial factor for practical extraction applications. To ensure the regenerability and the recyclability of the prepared carbon-ZrO_2-HF/PVDF membrane, the above described procedure was repeated 10 times for the extraction of the bisphenol A (**Fig. 7**). Between consecutive extractions, the membrane was washed with methanol (3 x 4 mL) and rinsed with pure water before reuse. The relative error in the measured absorbances was 2.0%, indicating the high reproducibility of the extraction procedure and the easy regeneration and excellent reusability of the prepared carbon-ZrO_2-HF/PVDF membranes for the extraction of bisphenol A.

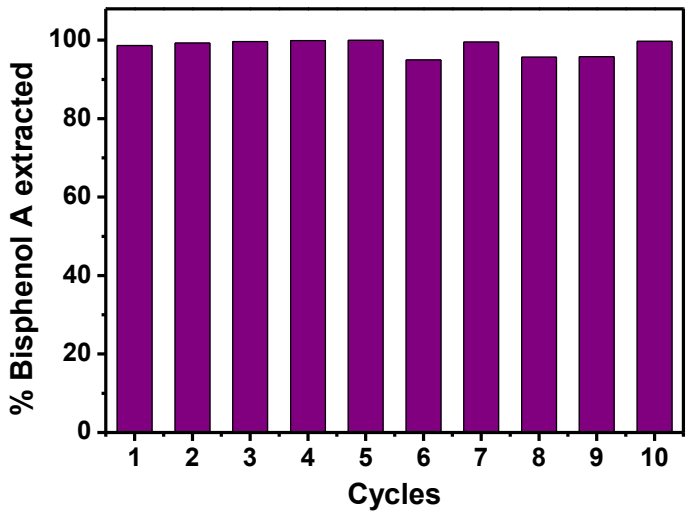

Fig. 7. Regenerability of carbon-ZrO_2-HF/PVDF membranes for adsorption of bisphenol A from water.

4. Conclusions

In summary, highly porous carbons have been prepared by carbonization of UiO-66 MOF in nitrogen atmosphere and subsequently treatment with hydrofluoric acid to obtain additional porosity. The obtained carbons were characterized and used as sorbents for the extraction of rhodamine B dye from water under batch conditions. The UiO-66 derived etched-carbon has demonstrated to be an effective adsorbent because of its high porosity and open pore network, which facilitates the access of the rhodamine B molecules to the pores, and for their high degree of graphitization of the carbon structure that allows π -π interactions with aromatic compounds. The prepared porous carbons were used for the preparation of membranes, which showed excellent flow-through properties, enabling the extraction of organic pollutants under dynamic conditions. The developed etched-carbon/polymer membranes showed high performance for removal of rhodamine B dye, being able to treat a high volume of the sample, and of different phenolic compounds, with an excellent recyclability. The results suggest that UiO-66-derived carbon-ZrO_2-

HF/PVDF membranes are very promising materials for flow-through of various environmental pollutants.

Acknowledgments

Spanish Agencia Estatal de Investigación (AEI) and the European Funds for Regional Development (FEDER) are gratefully acknowledged for financial support through Projects CTQ2013-47461-R and CTQ2016-77155-R (AEI/FEDER, UE). M. del Rio acknowledges the support from the Conselleria d'Innovació, Recerca i Turisme (pre-doctoral fellowship). The authors acknowledge F. Hierro Riu for scanning micrographs.

Supplementary data

Powder X-ray pattern, SEM image and adsorption isotherms of UiO-66 precursor MOF, nitrogen adsorption-desorption isotherms, pore size distribution, linear fit of pseudo-second order kinetics model for the adsorption of rhodamine B of carbon-ZrO_2 and carbon-ZrO_2-HF samples, detailed SEM images of carbon-ZrO_2-HF/PVDF composite and structure of the phenolic compounds extracted.

References

[1] H. Furukawa, K.E. Cordova, M. O'Keeffe, O.M. Yaghi, The chemistry and applications of metal-organic frameworks, Science 341 (2013) 123044–1230455.

[2] M. Eddaoudi, J. Kim, N. Rosi, D. Vodak, J. Wachter, M. O'Keeffe, O.M. Yaghi, Systematic design of pore size and functionality in isoreticular MOFs and their application in methane storage, Science 295 (2002) 469–472.

[3] G. Férey, Hybrid porous solids: past, present, future, Chem. Soc. Rev. 37 (2008) 191–214.
[4] N. Stock, S. Biswas, Synthesis of metal-organic frameworks (MOFs): Routes to various MOF topologies, morphologies, and composites, Chem. Rev. 112 (2012) 933–969.
[5] S.T. Meek, J.A. Greathouse, M.D. Allendorf, Metal-organic frameworks: A rapidly growing class of versatile nanoporous materials, Adv. Mater. 23 (2011) 249–267.
[6] A. Dhakshinamoorthy, H. Garcia, Metal-organic frameworks as solid catalysts for the synthesis of nitrogen-containing heterocycles, Chem. Soc. Rev. 43 (2014) 5750–5765.
[7] J. Gascon, A. Corma, F. Kapteijn, F.X. Llabrés i Xamena, Metal-organic framework catalysis: Quo vadis?, ACS Catal. 4 (2014) 361–378.
[8] Q.-G. Zhai, X. Bu, C. Mao, X. Zhao, P. Feng, Systematic and dramatic tuning on gas sorption performance in heterometallic metal-organic frameworks, J. Am. Chem. Soc. 138 (2016) 2524–2527.
[9] D. Banerjee, A.J. Cairns, J. Liu, R.K. Motkuri, S.K. Nune, C.A. Fernandez, R. Krishna, D.M. Strachan, P.K. Thallapally, Potential of metal-organic frameworks for separation of xenon and krypton, Acc. Chem. Res. 48 (2015) 211–219.
[10] L.E. Kreno, K. Leong, O.K. Farga, M. Allendorf, R.P. Van Duyne, J.T. Hupp, Metal-organic framework materials as chemical sensors, Chem. Rev. 112 (2012) 1105–1125.
[11] W. Cai, C.-C. Chu, G. Liu, Y.X. Wáng, Metal-organic framework-based nanomedicine platforms for drug delivery and molecular imaging, Small 11 (2015) 4806-4822.
[12] Z.-Y. Gu, C.-X. Yang, N. Chang, X.-P. Yan, Metal-organic frameworks for analytical chemistry: From sample collection to chromatographic separation, Acc. Chem. Res. 45 (2012) 734–745.
[13] N.A. Khan, Z. Hasan, S.H. Jhung, Adsorptive removal of hazardous materials using metal-organic frameworks (MOFs): A review, J. Hazard. Mater. 244-245 (2012) 444–456.
[14] F. Maya, C. Palomino Cabello, S. Clavijo, J.M. Estela, V. Cerdà, G. Turnes Palomino, Zeolitic imidazolate framework dispersions for the fast and highly efficient extraction of organic micropollutants, RSC Adv. 5 (2015) 28203–28210.
[15] B. Wang, X.-L. Lv, D. Feng, L.-H. Xie, J. Zhang, M. Li, Y. Xie, J.-R. Li, H.-C. Zhou, Highly stable Zr(IV)-based metal-organic frameworks for the detection and removal of antibiotics and organic explosives in water, J. Am. Chem. Soc. 138 (2016) 6204–6216.
[16] F. Maya, C. Palomino Cabello, R.M. Frizzarin, J.M. Estela, G. Turnes Palomino, V. Cerdà, Magnetic solid-phase extraction using metal-organic frameworks (MOFs) and their derived carbons, TrAC Trends Anal. Chem. 90 (2017) 142–152.
[17] W. Xia, A. Mahmood, R. Zou, Q. Xu, Metal-organic frameworks and their derived nanostructures for electrochemical energy storage and conversion, Energy Environ. Sci. (2015) 1837–1866.
[18] J. Shao, Z. Wan, H. Liu, H. Zheng, T. Gao, M. Shen, Q. Qu, H. Zheng, Metal organic frameworks-derived Co_3O_4 hollow dodecahedrons with controllable interiors as outstanding anodes for Li storage, J. Mater. Chem. A 2 (2014) 12194–12200.
[19] M. Hu, J. Reboul, S. Furukawa, N.L. Torad, Q. Ji, P. Srinivasu, K. Ariga, S. Kitagawa, Y. Yamauchi, Direct carbonization of Al-based porous coordination polymer for synthesis of nanoporous carbon, J. Am. Chem. Soc. 134 (2012) 2864–2867.
[20] J. Tang, R.R. Salunkhe, J. Liu, N.L. Torad, M. Imura, S. Furukawa, Y. Yamauchi, Thermal conversion of core-shell metal-organic frameworks: A new method for selectively functionalized nanoporous hybrid carbon, J. Am. Chem. Soc. 137 (2015) 1572–1580.
[21] K. Xi, S. Cao, X. Peng, C. Ducati, R.V. Kumar, A.K. Cheetham, Carbon with hierarchical pores from carbonized metal-organic frameworks for lithium sulphur batteries, Chem. Commun. 49 (2013) 2192–2194.
[22] W. Chaikittisilp, K. Ariga, Y. Yamauchi, A new family of carbon materials: synthesis of MOF-derived nanoporous carbons and their promising applications, J. Mater. Chem. A 1 (2013) 14–19.
[23] S.J. Yang, T. Kim, J. H. Im, Y.S. Kim, K. Lee, H. Jung, C.R. Park, MOF-derived hierarchically porous carbon with exceptional porosity and hydrogen storage capacity, Chem. Mater. 24 (2012) 464–470.
[24] X. Wang, J. Zhou, H. Fu, W. Li, X. Fan, G. Xin, J. Zheng, X. Li, MOF derived catalysts for electrochemical oxygen reduction, J. Mater. Chem. A 2 (2014) 14064–14070.
[25] Y.-Z. Chen, C. Wang, Z.-Y. Wu, Y. Xiong, Q. Xu, S.-H. Yu, H.-L. Jiang, From bimetallic metal-organic framework to porous carbon: High surface area and multicomponent active dopants for excellent electrocatalysis, Adv. Mater. 27 (2015) 5010–5016.
[26] N.L. Torad, M. Hu, S. Ishihara, H. Sukegawa, A.A. Belik, M. Imura, K. Ariga, Y. Sakka, Y. Yamauchi, Direct synthesis of MOF-derived nanoporous carbon with magnetic Co nanoparticles toward efficient water treatment, Small 10 (2014) 2096–2107.

[27] X. Liu, C. Wang, Q. Wu, Z. Wang, Metal-organic framework-templated synthesis of magnetic nanoporous carbon as an efficient adsorbent for enrichment of phenylurea herbicides, Anal. Chim. Acta 870 (2015) 67–74.
[28] X. Liu, C. Wang, Z. Wang, Q. Wu, Z. Wang, Nanoporous carbon derived from a metal organic framework as a new kind of adsorbent for dispersive solid phase extraction of benzoylurea insecticides, Microchim. Acta 182 (2015) 1903–1910.
[29] L. Hao, X. Liu, J. Wang, C. Wang, Q. Wu, Z. Wang, Use of ZIF-8-derived nanoporous carbon as the adsorbent for the solid phase extraction of carbamate pesticides prior to high-performance liquid chromatographic analysis, Talanta 142 (2015) 104–109.
[30] M. Li, J. Wang, C. Jiao, C. Wang, Q. Wu, Z. Wang, Magnetic porous carbon derived from a Zn/Co bimetallic metal-organic framework as an adsorbent for the extraction of chlorophenols from water and honey tea samples, J. Sep. Sci. 39 (2016) 1884–1891.
[31] R. Ma, L. Hao, J. Wang, C. Wang, Q. Wu, Z. Wang, Magnetic porous carbon derived from a metal-organic framework as a magnetic solid-phase extraction adsorbent for the extraction of sex hormones from water and human urine, J. Sep. Sci. 39 (2016) 3571–3577.
[32] B.N. Bhadra, S.H. Jhung, A remarkable adsorbent for removal of contaminants of emerging concern from water: Porous carbon derived from metal azolate framework-6, J. Hazard. Mater. 340 (2017) 179–188.
[33] Z. Hasan, D.-W. Cho, I.-H. Nam, C.-M. Chon, H. Song, Preparation of calcined zirconia-carbon composite from metal organic frameworks and its application to adsorption of crystal violet and salicylic acid, Materials 9 (2016) 261.
[34] M. Saraji, N. Mehrafza, Mesporous carbon-zirconium oxide nanocomposite derived from carbonized metal organic framework: A coating for solid-phase microextraction, J. Chromatrogr. A 1460 (2016) 33–39.
[35] J.H. Cavka, S. Jakobsen, U. Olsbye, N. Guillou, C. Lamberti, S. Bordiga, K.P. Lillerud, A new zirconium inorganic building brick forming metal organic frameworks with exceptional stability, J. Am. Chem. Soc. 130 (2008) 13850–13851.
[36] Y.S. Seo, N.A. Khan, S.H. Jhung, Adsorptive removal of methylchlorophenoxypropionic acid from water with a metal-organic framework, Chem. Eng. J. 270 (2015) 22–27.
[37] Z. Hasan, N.A. Khan, S.H. Jhung, Adsorptive removal of diclofenac sodium from water with Zr-based metal-organic frameworks, Chem. Eng. J. 284 (2016) 1406–1413.
[38] C. Wang, X. Liu, J.P. Chen, K. Li, Superior removal of arsenic from water with zirconium metal-organic framework UiO-66, Sci. Rep. 5 (2015) 16613.
[39] M. del Rio, C. Palomino Cabello, V. Gonzalez, F. Maya, J.B. Parra, V. Cerdà, G. Turnes Palomino, Metal oxide assisted preparation of core-shell beads with dense metal-organic framework coatings for the enhanced extraction of organic pollutants, Chem. Eur. J. 22 (2016) 11770–11777.
[40] A. Ahmed, M. Forster, R. Clowes, D. Bradshaw, P. Myers, H. Zhang, Tuning morphology of nanostructured ZIF-8 on silica microspheres and applications in liquid chromatography and dye degradation, ACS Appl. Mater. Interfaces 7 (2015) 18054–18063.
[41] M.M. Abolghasemi, V. Yousefi, Three dimensionally honeycomb layered double hydroxides framework as a novel fiber coating for headspace solid-phase microextraction of phenolic compounds, J. Chromatogr. A 1345 (2014) 9–16.
[42] S. Lirio, C.-W. Fu, J.-Y. Lin, M.-J. Hsu, H.-Y. Huang, Solid-phase microextraction of phthalate esters in water sample using different activated carbon-polymer monoliths as adsorbents, Anal. Chim. Acta 927 (2016) 55–63.
[43] Y. Lv, X. Tan, F. Svec, Preparation and applications of monolithic structures containing metal-organic frameworks, J. Sep. Sci. 40 (2017) 272–287.
[44] T. Wang, J. Wang, C. Zhang, Z. Yang, X. Dai, M. Cheng, X. Hou, Metal-organic framework MIL-101(Cr) as a sorbent of porous membrane-protected micro-solid-phase extraction for the analysis of six phthalate esters from drinking water: a combination of experimental and computational study, Analyst 140 (2015) 5308–5316.
[45] M. Ghani, M.F.F. Picó, S. Salehinia, C. Palomino Cabello, F. Maya, G. Berlier, M. Saraji, V. Cerdà, G. Turnes Palomino, Metal-organic framework mixed-matrix disks: Versatile supports for automated solid-phase extraction prior to chromatographic separation, J. Chromatogr. A 1488 (2017) 1–9.
[46] S.D. Richardson, Water analysis: emerging contaminants and current issues. Anal. Chem. 81 (2009) 4645–4677.
[47] S.J. Garibay, S.M. Cohen, Isoreticular synthesis and modification of frameworks with the UiO-66 topology, Chem. Commun. 46 (2010) 7700–7702.

[48] M.S. Denny, S.M. Cohen, In situ modification of metal-organic frameworks in mixed-matrix membranes, Angew. Chem. Int. Ed. 54 (2015) 9029–9032.
[49] Y.S. Ho, G. McKay, Pseudo-second order model for sorption processes, Process Biochem. 34 (1999) 451–465.
[50] Y.S. Ho, Second-order kinetic model for the sorption of cadmium onto tree fern: A comparison of linear and non-linear methods, Water Res. 40 (2006) 119–125.
[51] Q. Flamant, M. Anglada, Hydrofluoric acid etching of dental zirconia. Part 2: effect on flexural strength and ageing behavior, J. Eur. Ceram. Soc. 36 (2016) 135–145.
[52] W. Cao, W. Luo, H. Ge, Y. Su, A. Wang, T. Zhang, UiO-66 derived Ru/ZrO2@C as a highly stable catalyst for hydrogenation of levulinic acid to □-valerolactone, Green Chem. 19 (2017) 2201–2211.
[53] M.T. Yagub, T.K. Sen, S. Afroze, H.M. Ang, Dye and its removal from aqueous solution by adsorption: A review, Adv. Colloid Interface Sci. 209 (2014) 172–184.
[54] P.P. Selvam, S. Preethi, P. Basakaralingam, N. Thinakaran, A. Sivasamy, S. Sivanesan, Removal of rhodamine B from aqueous solution by adsorption onto sodium montmorillonite, J. Hazard. Mater. 155 (2008) 39–44.
[55] L. Li, S. Liu, T. Zhu, Application of activated carbon derived from scrap tires for adsorption of Rhodamine B, J. Environ. Sci. 22 (2010) 1273–1280.
[56] J. Anandkumar, B. Mandal, Adsorption of chromium(VI) and Rhodamine B by surface modified tannery waste: Kinetic, mechanistic and thermodynamic studies, J. Hazard. Mater. 186 (2011) 1088–1096.
[57] H. Mittal, S.B. Mishra, Gum ghatti and Fe_3O_4 magnetic nanoparticles based nanocomposites for the effective adsorption of rhodamine B, Carbohydr. Polym. 101 (2014) 1255–1264.
[58] M.-F. Hou, C.-X. Ma, W.-D. Zhang, X.-Y. Tang, Y.-N. Fan, H.-F. Wan, Removal of rhodamine B using iron-pillared bentonite, J. Hazard. Mater. 186 (2011) 1118–1119.
[59] Y. Guo, J. Zhao, H. Zhang, S. Yang, J. Qi, Z. Wang, H. Xu, Use of rice husk-based porous carbon for adsorption of Rhodamine B from aqueos solutions, Dyes Pigments, 66 (2005) 123–128.
[60] Q.-S. Liu, T. Zheng, P. Wang, J.-P. Jiang, N. Li, Adsorption isotherm, kinetic and mechanism studies of some substituted phenols on activated carbon fibers, Chem. Eng. J. 157 (2010) 348–356.